Available online at www.sciencedirect.com
ScienceDirect
Physics Letters A 370 (2007) 449–453
PHYSICS LETTERS A
www.elsevier.com/locate/pla

Signal amplification in NbN superconducting resonators via stochastic resonance

Baleegh Abdo *, Eran Segev, Oleg Shtempluck, Eyal Buks

Microelectronics Research Center, Department of Electrical Engineering, Technion, Haifa 32000, Israel

Received 1 April 2007; received in revised form 27 May 2007; accepted 31 May 2007

Available online 6 June 2007

Communicated by A.R. Bishop

Abstract

We exploit nonlinearity in NbN superconducting stripline resonators, which originates from local thermal instability, for studying stochastic resonance. As the resonators are driven into instability, small amplitude modulation (AM) signals are amplified with the aid of injected white noise. Simulation results based on the equations of motion for the system yield a good agreement with the experimental data both in the frequency and time domains.

Keywords: Nonlinear resonators; Superconducting devices; Stochastic processes

The notion that certain amount of white noise can appreciably amplify small periodic modulating signals acting on bistable systems, generally known as *stochastic resonance* (SR), has been over the last two decades of a great interest [1–4]. It has been applied for instance to account for the periodicity of ice ages occurring on earth [5], as well as to explain some important neurophysiological processes [6]. Furthermore, it has been used to amplify small signals in various nonlinear systems, e.g. the intensity of one laser mode in a bistable ring laser [7], the magnetic flux in a superconducting quantum interference device [8], and even more recently, a small periodic drive of a nanomechanical oscillator [9,10]. The performance of an amplifier based on SR strongly depends in general on the underlying mechanism responsible for nonlinear instability. Here we employ a novel thermal instability mechanism, which has been recently discovered in superconducting NbN microwave resonators [11], to study SR. Contrary to other systems, which were employed before for studying SR, the dynamics in the present case is piecewise linear [12]. Moreover, the correlation time of the dynamical variable, which triggers transitions between metastable states, namely the temperature, is finite in our system [13]. These unique properties give rise to extreme nonlinearity, which occurs at a relatively low power level [14]. As we demonstrate in this Letter, both experimentally and theoretically, this mechanism is highly suitable for achieving high gain amplification at a relatively low power level.

In the experiment the resonators are driven into instability using a microwave pump having a frequency, which lies within the resonance band of the system. The amplified signal in this scheme is a small amplitude modulation (AM) drive modulating the pump signal with a relatively low frequency.

The superconducting resonator is fabricated in stripline geometry while using Sapphire as a dielectric material. The layout of the center conductor implemented is shown at the top-right corner of Fig. 2. Fabrication details as well as nonlinear characterization of such resonators can be found in Ref. [11].

In order to set a possible working point of the resonator at the metastable region, two preliminary hysteresis measurements were performed. In one measurement exhibited in Fig. 1(a), forward and backward frequency sweeps of the reflection parameter S_{11}, measured for the resonator fundamental mode at $f_0 \simeq 2.57\,\mathrm{GHz}$, reveal two hysteresis loops at both sides of the resonance line shape at which the resonator becomes bistable. In another measurement shown in Fig. 1(b) the frequency of the pump f_p was set to 2.565 GHz positioned at the left side of the

* Corresponding author.
E-mail address: baleegh@tx.technion.ac.il (B. Abdo).

0375-9601/$ – see front matter
doi:10.1016/j.physleta.2007.05.103

resonance, while the input power was swept in the forward and the backward directions. A hysteresis loop of the reflection parameter appears in this measurement as well, this time along the power axis. Thus, the working point was set to $f_p = 2.565\,\text{GHz}$, $P_0 = -21.5\,\text{dBm}$, while the applied modulation drive is a sinusoidal AM signal with a modulation amplitude $A_{\text{mod}} = 0.27$.

A schematic diagram of the experimental setup employed in the measurement of SR is depicted in Fig. 2. A coherent signal $P_0 \cos(\omega_p t)$ with angular frequency $\omega_p = 2\pi f_p$ is AM modulated using a sinusoidal generator with an angular frequency Ω. The modulated signal is combined with a white noise and injected into the resonator. The white noise, which is generated using a noise source is amplified using an amplifying stage and tuned via an adjustable attenuator. Thus, the input signal power fed to the feedline of the resonator (after calibrating the path losses) reads

$$P_{\text{in}}(t) = P_0\big[1 + A_{\text{mod}} \sin(\Omega t + \varphi)\big] \cos(\omega_p t) + \xi(t), \tag{1}$$

where $\xi(t)$ denotes a zero-mean Gaussian white noise $\langle \xi(t) \rangle = 0$, with autocorrelation function $\langle \xi(t)\xi(t') \rangle = 2D\delta(t - t')$, where D is the noise intensity. Whereas, the reflected power off the resonator is mixed with a local oscillator with frequency f_p and measured simultaneously in the time and frequency domains using an oscilloscope and a spectrum analyzer respectively.

It is worthwhile to point out here that the SR phenomenon excited by means of AM modulation (Eq. (1)), can be considered as well as a high-frequency stochastic resonance of the kind defined by Dykman et al. [15] and demonstrated experimentally by Chan and Stambaugh [16] on nanomechanical oscillators, where the frequencies of the weak modulating drive $\omega_p \pm \Omega$ lie close to the frequency of the main periodic driving force ω_p.

Furthermore, for small amplitudes of the modulation signal $A_{\text{mod}} \ll 1$ and in steady state conditions, the spectral density of the reflected power at the output of the homodyne setup, can in general be written in the form [3,4]

$$S(\omega) = 2\pi P_0^r \delta(\omega) + \pi \sum_{n=1}^{\infty} A_n^r(D)\big[\delta(\omega - n\Omega) + \delta(\omega + n\Omega)\big] + S_N(\omega), \tag{2}$$

which is composed of a delta spike at dc ($\omega = 0$), delta spikes with amplitudes $A_n^r(D)$ centered at $\omega = \pm n\Omega$, $n = 1, 2, 3, \ldots$, and a background spectral density of the noise denoted by $S_N(\omega)$. Whereas P_0^r designates the dc component of the reflected power.

As it is known, one of the distinguished fingerprints of SR phenomenon is a peak observed in the signal to noise ratio (SNR) curve as a function of the input noise intensity D, corresponding to some nonzero intensity D_{SR}. This counterintuitive amplification in SNR curve is generally explained in terms of coherent interaction between the modulating signal and the stochastic noise entering the system.

In this framework the SNR for the nth harmonic can be defined as [1]

$$\text{SNR}_n \equiv 2\pi A_n^r(D)/S_N(n\Omega), \tag{3}$$

where SNR of the fundamental harmonic corresponds to $n = 1$.

In Fig. 3(a) and (b), two SNR data curves (blue) are drawn as a function of the noise intensity, corresponding to the odd harmonics $n = 3$ and $n = 5$ respectively. Both curves display a synchronized peak in the SNR around D_{SR} of 0.94 fW/Hz.

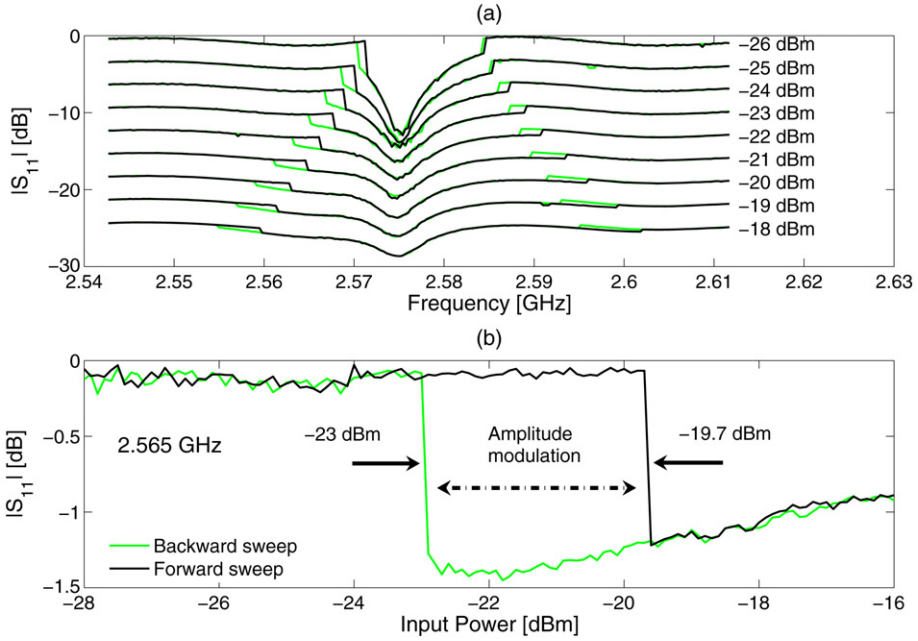

Fig. 1. (Color online.) (a) Forward and backward frequency sweeps applied to the first mode of the resonator at ∼2.57 GHz. The sweeps exhibit hysteresis loops at both sides of the resonance line shape. The plots which correspond to different input powers were shifted by a vertical offset for clarity. (b) Reflected power hysteresis measured at a constant angular frequency $\omega_p = 2\pi \times 2.565$ GHz which resides within the left-side metastable region of the resonance. For both plots the black (dark) line represents a forward sweep whereas the green (light) line represents a backward sweep.

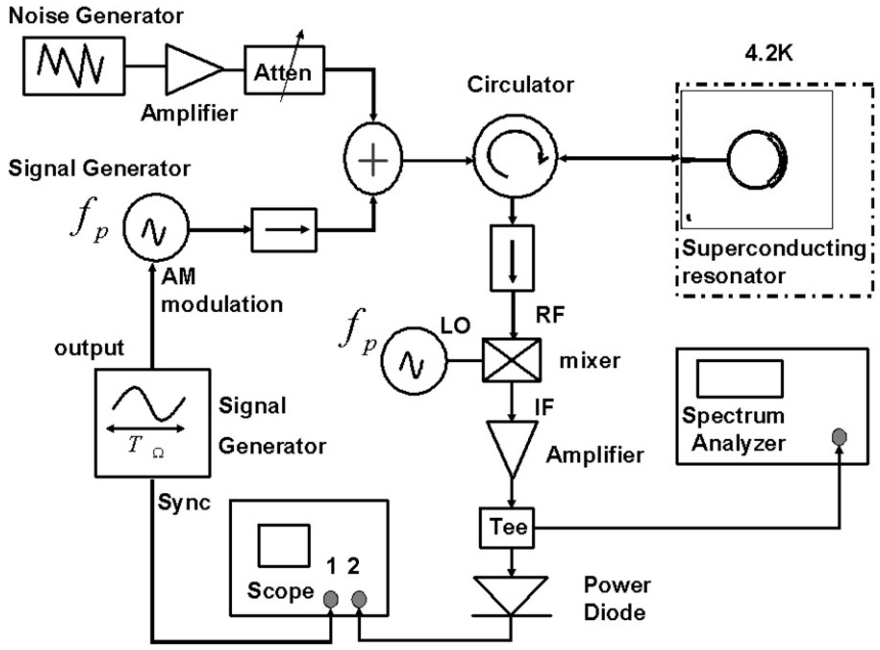

Fig. 2. Schematic drawing of the experimental setup used to measure SR. The microwave signal generator and the local oscillator at frequency f_p were phase-locked. The layout of the resonator is shown at the top-right corner.

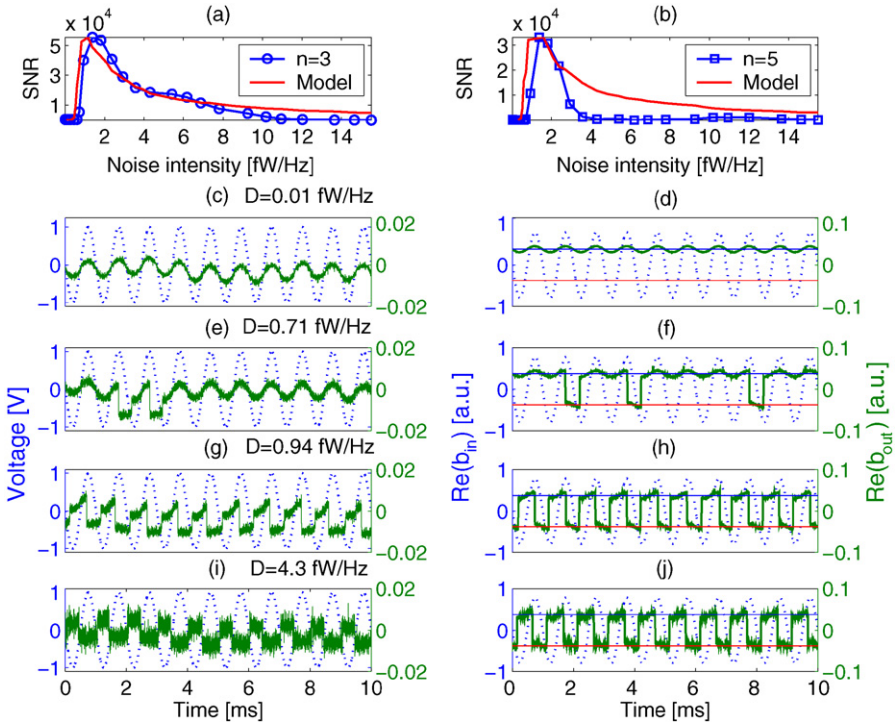

Fig. 3. (Color online.) Panels (a) and (b) show measured (blue) and simulated (red) SNR curves of the output harmonics $n = 3$ and $n = 5$ as a function of the input noise intensity. Panels (c), (e), (g) and (i) at the left exhibit typical snapshots of the reflected signal measured in the time domain as the input noise intensity D is increased. While panels (d), (f), (h) and (j) show the corresponding simulation results. Panels (c)–(d) and (e)–(f) correspond to noise intensities below D_{SR}. Panels (g)–(h) correspond to a noise intensity of $D_{\mathrm{SR}} = 0.94$ fW/Hz. Panels (i)–(j) correspond to noise intensities higher than D_{SR}. The dotted sinusoidal blue line represents the modulation signal. While the upper (blue) and lower (red) constant lines plotted in the simulation results represent the steady state solution of the resonator in the (S) and (N) phases of the hot spot. The simulation parameters used are: $\omega_{0n} = 2\pi \times 2.57$ GHz, $\omega_{0s}/\omega_{0n} = 1.002$, $\gamma_{1s}/\omega_{0n} = 1.1 \times 10^{-3}$, $\gamma_{2s}/\omega_{0n} = 2.7 \times 10^{-3}$, $\gamma_{1n}/\omega_{0n} = 10^{-3}$, $\gamma_{2n}/\omega_{0n} = 2 \times 10^{-3}$, $\omega_p/\omega_{0n} = 0.9991$, $(b^{\mathrm{in}})^2/\omega_{0n} = 9 \times 10^9$, $\Omega/2\pi = 1$ kHz, $T_0 = 4.2$ K, $T_c = 10.7$ K, $C = 1.2 \times 10^{-12}$ J/K, $H = 3 \times 10^{-5}$ W/K.

The data of the first harmonic (not shown here) exhibit an SNR peak of 2×10^5 at D_{SR}.

Typical results of SR measured in the time domain are shown in the left panels of Fig. 3. Panels (c) and (e) correspond to

low noise levels below D_{SR}. Panel (c) shows the reflected sinusoidal at $\Omega/2\pi = 1$ kHz without jumps. Panel (e) shows the reflected sinusoidal containing a few arbitrary jumps. Whereas, panel (g) which corresponds to the resonance noise D_{SR} exhibits one jump in the reflected signal at every half cycle. Thus, satisfying generally the *time-scale matching condition* for SR given by $\tau(D_{SR}) = T_\Omega/2$, where $T_\Omega = 2\pi/\Omega$ and $\tau(D)$ is the metastable state lifetime corresponding to the noise intensity D [1]. In panel (i) on the other hand, the case of a noise level higher than D_{SR} is shown at which the coherence between the modulating drive and the noise is lost and the noise fluctuations almost completely screen the signal.

In order to retrieve the experimental results observed in the time and frequency domains shown in Fig. 3, we employ the theoretical model elaborated in [13], according to which, the nonlinear dynamics exhibited by the system can be described to a large extent using two coupled equations of motion, one for the slowly varying amplitude of the resonator mode B given by

$$\frac{dB}{dt} = \left[i(\omega_p - \omega_0) - \gamma\right]B - i\sqrt{2\gamma_1}b^{in} + c^{in}, \tag{4}$$

and the other for the hot spot temperature T (the model assumes one dominant hot spot) which reads

$$C\frac{dT}{dt} = Q - W, \tag{5}$$

where ω_0 is the angular resonance frequency, b^{in} is the amplitude of the coherent tone injected to the resonator feedline $b^{in}e^{-i\omega_p t}$, $\gamma = \gamma_1 + \gamma_2$, where γ_1 is the coupling factor between the resonator and the feedline, γ_2 is the damping rate of the mode, C is the thermal heat capacity, $Q = \hbar\omega_0 2\gamma_2|B|^2$ is the power heating up the hot spot, $W = H(T - T_0)$ is the power of the heat transfer to the coolant which is assumed to be at temperature T_0, while H is the heat transfer coefficient. The term c^{in} represents an input noise with a random phase $\langle c^{in}\rangle = 0$ and an autocorrelation function $\langle c^{in}(t)c^{in*}(t')\rangle = G\omega_0\delta(t - t')$, where $G = \gamma D/\hbar\omega_0^2$. Whereas in order to obtain the reflected signal $b^{out}e^{-i\omega_p t}$ the following input–output relation is used [13]

$$b^{out} = b^{in} - i\sqrt{2\gamma_1}B. \tag{6}$$

Furthermore, this model assumes a step function dependence of the resonator parameters $\omega_0, \gamma_1, \gamma_2$ on the hot spot temperature T. As T exceeds the critical temperature T_c (the hot spot in the normal (N) phase) the resonator is characterized by ω_{0n}, γ_{1n}, γ_{2n}, while in the complementary case where $T \leqslant T_c$ (the hot spot in the superconducting (S) phase), these parameters equal ω_{0s}, γ_{1s}, γ_{2s}.

Due to the dependence of the stored energy inside the resonator on the resonance frequencies and the damping rates of the resonator, and the dependence of these parameters on the temperature of the hot spot, the system may have, in general, up to two locally-stable steady states, corresponding to the S and N phases of the hot spot. The stability of each of these phases depends on both the power and frequency parameters of the injected pump tone. In general there exist four different stability

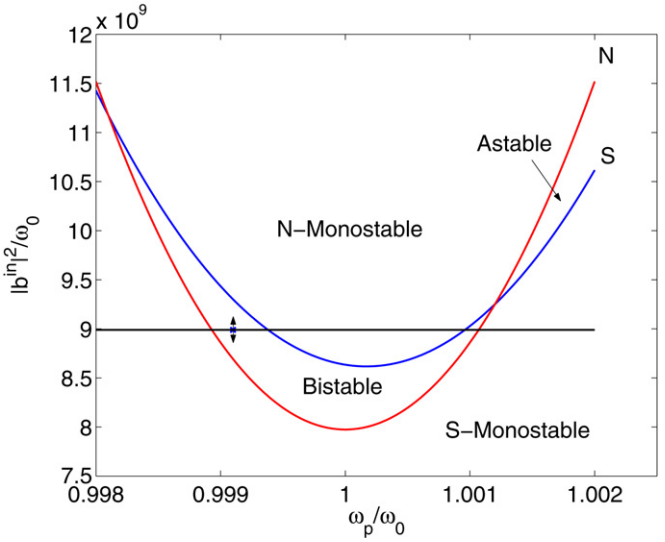

Fig. 4. (Color online.) Stability diagram showing the stability zones of the simulated nonlinear system as a function of the injected pump power and frequency. The red and blue lines in the figure denoted by N and S represent respectively the threshold of the N and S states, which consequently divides the pump power-frequency plane into four stability zones. Two are monostable zones, where either the S phase or the N phase is locally stable. Another is a bistable zone, where both phases are locally stable. The third is an astable zone, where none of the phases are locally stable. The working point employed in the simulation is indicated by a small cross drawn within the bistable region, while the vertical double arrow passing through this point illustrates the operation of an AM modulation. The various model parameters employed in the simulation are listed in the caption of Fig. 3.

zones [17] (see Fig. 4). Two are monostable zones, where either the S phase or the N phase is locally stable. Another is a bistable zone, where both phases are locally stable. The third is an astable zone, where none of the phases are locally stable. Consequently, by setting the average value of $(b^{in})^2$ (which is proportional to the pump power) such that the system is located within the bistable region (see Fig. 4), and further determining an appropriate small amplitude ac component (which represents the signal with frequency Ω), one gets the theoretical fit lines (red) plotted in Fig. 3(a) and (b). Thus, apart from the y-axis scaling factor applied to coincide the SNR peaks with those of the data, the model, despite its simplicity, yields a relatively good agreement with the experimental data. Likewise, a good agreement is obtained also in the time domain, where the time simulations (d), (f), (h), (j) are drawn at the right of the corresponding measurement results. The constant upper (blue) and lower (red) lines shown in these panels correspond to the steady state of the resonator (hot spot) in the S and N phases respectively. It is worthwhile mentioning that some of the model parameters applied in the simulation (listed in the caption of Fig. 3) were measured directly (ω_{0n}, ω_{0s}, T_0, T_c, $\Omega/2\pi$, ω_p), whereas others were set to typical values characterizing superconducting nonlinear resonators made of NbN (γ_1, γ_2, C, H) [11].

Moreover, by inspecting the time response of the measurement results mainly panels (g) and (i), we find that the reflected modulated signals exhibit a rather rectangular shape. Such distortion of the sinusoidal shape at the output is very likely to originate from the dispersive character of the system response

as was suggested in Refs. [4,18]. Furthermore, by comparing these experimental data to the simulation plots exhibited in panels (h) and (j), one can verify that the suggested theoretical model manages to reproduce this feature as well.

In conclusion, nonlinear NbN superconducting resonators have been shown to exhibit SR when driven into the bistable region. Simulations based on the thermal instability model of the system succeeds to reproduce most of the measured SR features. Moreover, amplification of a slowly varying AM signal carried by a microwave pump is shown to be feasible by establishing a resonant cooperation between the modulating signal and the injected stochastic noise. Hence, such amplification scheme may be applicable in communication area. Namely, amplifying weak AM signals modulating a high frequency carrier [19] (located within the resonator metastable region), by means of tuning the input noise. Though to some extent, the range of possible application in this area might be limited by the nonlinearity of this amplification mechanism.

Acknowledgements

This work was supported by the German Israel Foundation under grant 1-2038.1114.07, the Israel Science Foundation under grant 1380021, the Deborah Foundation, the Poznanski Foundation, the Russel Berrie nanotechnology institute, and MAFAT.

References

[1] L. Gammaitoni, P. Hänggi, P. Jung, F. Marchesoni, Rev. Mod. Phys. 70 (1998) 223;
L. Gammaitoni, F. Marchesoni, S. Santucci, Phys. Rev. Lett. 74 (1995) 1052.
[2] A.R. Bulsara, L. Gammaitoni, Phys. Today (March 1996) 39.
[3] P. Jung, P. Hänggi, Phys. Rev. A 44 (1991) 8032.
[4] M. Morillo, J. Gómez-Ordóñez, Phys. Rev. E 51 (1995) 999.
[5] R. Benzi, A. Satera, G. Parisi, A. Vulpiani, J. Phys. A 14 (1981) L453;
R. Benzi, et al., SIAM J. Appl. Math. 43 (1983) 565.
[6] A. Longtin, A. Bulsara, F. Moss, Phys. Rev. Lett. 67 (1991) 656;
J.E. Levin, J.P. Miller, Nature 380 (1996) 165.
[7] B. McNamara, K. Wiesenfeld, R. Roy, Phys. Rev. Lett. 60 (1988) 2626;
R. Rouse, S. Han, J.E. Lukens, Appl. Phys. Lett. 66 (1995) 108.
[8] A.D. Hibbs, A.L. Singsaas, E.W. Jacobs, A.R. Bulsara, J.J. Pekkedahl, F. Moss, J. Appl. Phys. 77 (1995) 2582.
[9] R.L. Badzey, P. Mohanty, Nature 437 (2005) 995.
[10] R. Almog, S. Zaitsev, O. Shtempluck, E. Buks, Appl. Phys. Lett. 90 (2007) 013508.
[11] B. Abdo, E. Segev, O. Shtempluck, E. Buks, IEEE Trans. Appl. Supercond. 16 (2006) 1976;
B. Abdo, et al., Phys. Rev. B 73 (2006) 134513.
[12] M. Bier, R.D. Astumian, Phys. Rev. Lett. 71 (1993) 1649;
M. Bier, R.D. Astumian, Phys. Lett. A 247 (1998) 385.
[13] B. Abdo, E. Segev, O. Shtempluck, E. Buks, J. Appl. Phys. 101 (2007) 083909.
[14] E. Segev, B. Abdo, O. Shtempluck, E. Buks, Phys. Lett. A 366 (2007) 160.
[15] M.I. Dykman, D.G. Luchinsky, R. Mannella, P.V.E. McClintock, N.D. Stein, N.G. Stocks, Phys. Rev. E 49 (1994) 1198;
M.I. Dykman, D.G. Luchinsky, P.V.E. McClintock, N.D. Stein, N.G. Stocks, JETP Lett. 58 (1993) 145.
[16] H.B. Chan, C. Stambaugh, Phys. Rev. B 73 (2006) 224301;
H.B. Chan, C. Stambaugh, Phys. Rev. B 73 (2006) 172302.
[17] E. Segev, B. Abdo, O. Shtempluck, E. Buks, J. Phys.: Condens. Matter 19 (2007) 096206.
[18] M.I. Dykman, D.G. Luchinsky, R. Mannella, P.V.E. McClintock, N.D. Stein, N.G. Stocks, J. Stat. Phys. 70 (1993) 463.
[19] M. Golio (Ed.), The RF and Microwave Handbook, CRC Press, 2001.